Asian Pub. Corp.

www.asianpubs.org

ARTICLE

Effects of Different Carbonized Temperature on Photocatalytic Activity of TiO_2/C Hybrid Aerogels

Xia Shao[1], Zhili Zhang[2], Rui Zhang[1,✉] and Donghui Chen[2]

Asian Journal of Materials Chemistry

Volume: 2 Year: 2017
Issue: 2 Month: April-June
pp: 79–86
DOI: https://doi.org/10.14233/ajmc.2017.AJMC-P41

Received: 6 May 2017
Accepted: 1 June 2017
Published: 5 July 2017

ABSTRACT

The effect of carbonization temperature during the sol-gel preparation of TiO_2/C hybrid aerogels on their photocatalytic performance for degradation of methylene blue and methyl orange is investigated. XRD, SEM, TEM, N_2 adsorption, XPS and UV-visible spectroscopy were used to characterize the physico-chemical properties of TiO_2/C hybrid aerogels. Results showed that higher carbonization temperature can promote the growth of TiO_2/C nanoparticles in sol-gel process. Thereby, the porous properties, adsorption equilibrium and kinetics for methylene blue adsorption, crystalline size and band gap of TiO_2 in the hybrid aerogels are changed accordingly. The photocatalytic activity of the hybrid aerogels is dominantly determined by adsorption equilibrium and kinetics. The narrowness of the band-gap and light availability are also responsible for the high photocatalytic activity.

KEYWORDS

Photocatalysts, Degradation, Methylene blue, Methyl orange, Sol-gel method.

INTRODUCTION

Nowadays water pollution, caused by dye wastewater, is a serious problem. Dyes are widely used in textile, cosmetics and other industries. Effluents from these industries have high contents of organic pollutants, salts, chemical oxygen demand and suspended solids. Titanium dioxide (TiO_2) as a typical n-type semi-conductive photocatalyst for oxidation reactions has attracted much attention because of the potential applications in air purification, water treatment and other industries [1,2]. Because of the non-toxicity, strong oxidizing power, stablility to light irradiation [3-5] and low cost, TiO_2 has been regarded as one of the most promising photocatalysts among various photocatalysts. However, there are some disadvantages *e.g.*, TiO_2 has a wide band gap (3.2 eV), which limits its application in UV light range of solar spectrum. In addition, the recombination of photogenerated electron-hole pairs leads to a lowered photo-quantum efficiency of TiO_2 [6-8]. In order to solve these problems so that the photocatalytic properties of TiO_2 can be better utilized, it is necessary to modify the optical and electronic properties of TiO_2 to make it work under visible light. In case of the non-metal species, the synthesis of C-doped TiO_2 has raised great interest and become one of the most

Author affiliations:

[1]School of Materials Science and Engineering, Shanghai Institute of Technology, Shanghai, P.R. China
[2]School of Chemical and Environmental Engineering, Shanghai Institute of Technology, Shanghai, P.R. China

✉To whom correspondence to be addressed:

E-mail: sx961139@gmail.com

Available online at: http://ajmc.asianpubs.org

studied approaches to red shift of the light absorption [9-12]. This article focuses on preparation of TiO_2/C hybrid aerogels by changing carbonization temperature, in order to improve their photocatalytic effect to common dye wastewater, such as methylene blue.

In this work, we use $TiCl_4$ as TiO_2 source, resorcinol and furfural as carbon source to prepare TiO_2/C hybrid aerogels and the effects of carbonization temperature on the microstructure and performance of the synthesized hybrid aerogel catalysts were investigated. Their catalytic performance for methylene blue degradation was connected with the carbonization temperature in carbonized process and the microstructure of the aerogels.

EXPERIMENTAL

Resorcinol and furfural were purchased from Shanghai Ling Feng Chemical Reagent Co. Ltd. Titanium tetrachloride ($TiCl_4$), epoxypropane, methylene blue and absolute ethyl alcohol were purchased from Sinopharm Chemical Reagent Co Ltd. All chemicals were of analytical grade and used without further purification.

Aerogel preparation: TiO_2/C hybrid aerogels were obtained by a one-pot sol-gel method, followed by supercritical drying and carbonization, using resorcinol (R) and furfural (F) as carbon sources and $TiCl_4$ as the TiO_2 precursor. The molar ratio of propylene oxide to titanium is 6, the molar ratio of ethyl acetoacetate to Ti is 0.6 and the molar ratio of resorcinol to furfural is 1:2. The total mass of resorcinol and furfural is 10 g and $TiCl_4$ equivalent to TiO_2 of 3.80 g is 9.03 g. Resorcinol and furfural were added to a certain quality of absolute ethanol under magnetic stirring until a clear solution A was formed. Ethyl acetoacetate and another part of absolute ethanol according to the total volume of final solution of 100 mL was mixed to form a mixture solvent, to which $TiCl_4$ was added drop-wise in an ice bath under magnetic stirring, followed by propylene oxide addition to obtain a solution B. In an ice bath and magnetic stirring the solution A was added drop-wise to the solution B and the stirring was continued until the solution is clear and transparent. After the solution was dispensed in vial, sealed, standing 1-2 days at room temperature, it was placed in a water bath at 70 °C for 6 days to get a brown organic-inorganic wet hybrid gel.

The wet gel after aging was placed in propylene oxide solvent exchange for 7 days. After solvent exchange wet gel was then placed in an autoclave, with *n*-hexane as a supercritical drying medium. The TiO_2/resorcinol-furfural (RF) hybrid aerogels were carbonized at high temperature in a vertical furnace, under pure nitrogen atmosphere with a 5 °C /min heating rate and the carbonization temperature of 600 °C , 700 °C , 800 °C and 900 °C for 3 h to obtain four TiO_2/C hybrid aerogels.

Characterization: The phase structure and phase purity of the synthesized TiO_2 were examined by XRD, using a D/MAX 2000/PC diffractometer (Rigaku, Japan) with CuK_α radiation. Transmission electron microscope (TEM) and scanning electron microscope (SEM) images were collected by using a JEM 2010 EX microscope (JEOL, Japan) and a Scanning Electron Microscope Quanta 200 FEG (FEI Co., USA) with accelerating voltages of 30 and 200 K eV, respectively. Surface areas of samples were determined by applying adsorption data of p/p^0 between 0.01 and 0.26 to the Brunauer Emmett Teller (BET) equation. XPS spectra were recorded on an ESCALAB250Xi X-ray photoelectron spectrometer (Thermo Fisher Scientific, USA) using AlK_α radiation (1486.6 eV) and operating at 150 W.

Adsorption properties and photodegradation test: The photocatalytic activity of all the samples was evaluated *via* the photochemical reaction. Visible light source is 500 W xenon lamp. The methylene blue adsorption was performed in dark before light irradiation. The photochemical reaction was carried out as follows. 30 mg sample was added to a quartz tube, into which 50 mL methylene blue solution (20 mg/L) poured. The solution was stirred in the dark for 30 min to achieve the adsorption-desorption equilibrium. Then visible light was switched on for irradiation and 5 mL suspension was taken from the solution every 15 min for analysis by a pipette. The solution in the pipette was filtered (13 mm × 0.45 μm) and the absorbance at 285 nm of the was measured by a TU1810 UV-visible spectrophotometer.

RESULTS AND DISCUSSION

Characterization of the TiO_2/C hybrid aerogels: Fig. 1 shows the X-ray diffraction patterns of the TiO_2/C hybrid aerogels calcined at different temperatures. All the identified peaks can be assigned to the tetragonal structure of anatase TiO_2. The major peaks at 2θ values of 25.3°, 37.9°, 48.0°, 53.8° and 62.5° correspond to the (101), (004), (200), (105) and (204) planes, respectively [13]. No other crystalline impurities are detected, demonstrating that the products are composed of a single phase anatase TiO_2, despite of the heat treatment at 900 °C for 3 h. This phenomenon of inhibiting anatase TiO_2 transform to rutile TiO_2 at high temperature has been observed by many researchers [14-16] and probably caused by the interaction of TiO_2 and carbon. Then C is present in an amorphous state.

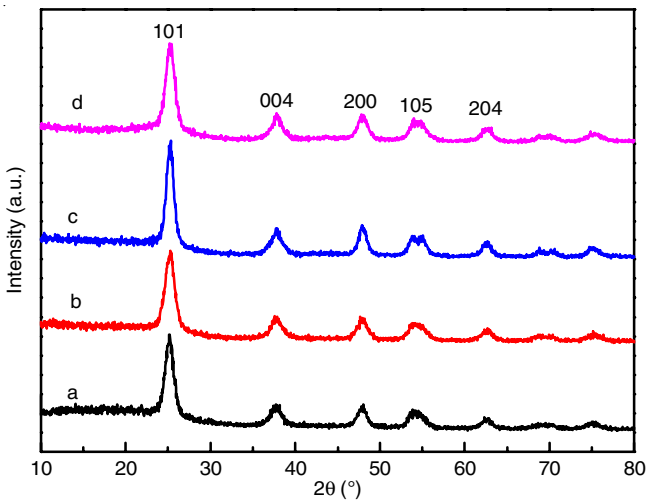

Fig. 1. X-ray diffraction patterns of the samples carbonized at different temperatures (a: TiO_2/C-600; b: TiO_2/C-700; c: TiO_2/C-800; d: TiO_2/C-900)

Based on the XRD data, the average crystallite sizes of TiO_2/C photocatalysts are calculated using the Debye-Scherrer equation and the results are shown in Table-1. It reveals that

TABLE-1
CRYSTALLITE SIZE OF SAMPLES CARBONIZED AT DIFFERENT TEMPERATURES

Samples	FWHM (°)	Crystallite size (nm)
TiO_2/C-600	1.170	6.877
TiO_2/C-700	1.074	7.499
TiO_2/C-800	0.950	8.470
TiO_2/C-900	0.647	12.440

the crystallite size increases from 6.877 to 12.44 nm with the increasing carbonization temperature, indicating that the carbonization temperature can accelerate the growth of crystalltie.

The SEM images of the synthesized TiO_2/C hybrid aerogels carbonized at different temperatures are shown in Fig. 2. It can be observed that all the samples obtained are highly porous material having a granular morphology with slight particle agglomeration and a relatively uniform particle diameter distribution. Meanwhile, the TiO_2/C-900 hybrid aerogels presents the most uniformity particles.

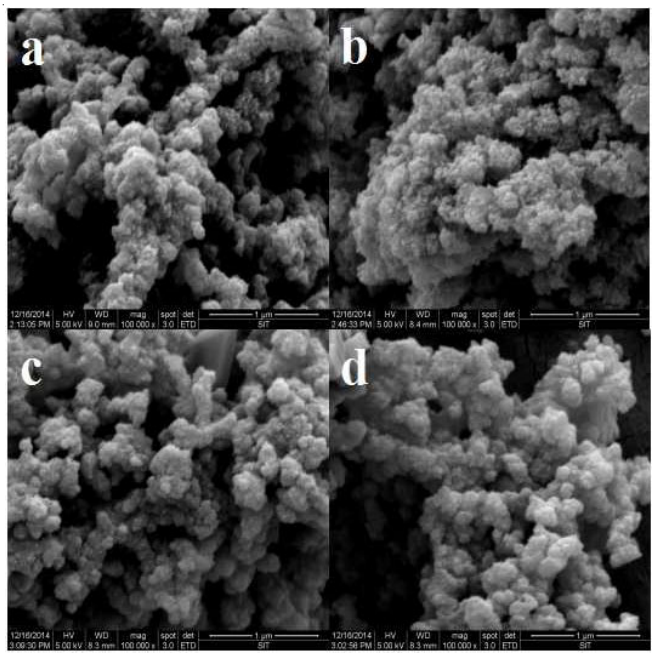

Fig. 2. SEM of the samples (a: TiO_2/C-600; b: TiO_2/C-700; c:TiO_2/C-800; d:TiO_2/C-900)

Fig. 3 shows the TEM images of the synthesized samples. It is observed that the TiO_2 nanoparticles are uniformly embedded in the substrates consisted by amorphous carbons, in which TiO_2 nanoparticles have a dark colour due to a high electron density of Ti element. This is the exact TiO_2/C hybrid aerogels what we needed. At the same time it is also observed that as the carbonization temperature rising, TiO_2 nanoparticles' size increases. This agrees well with the XRD results.

N_2 adsorption is carried out to characterize the textural properties of the aerogels. The specific surface areas (S_{BET}) and pore size distributions are determined by the Brunauer-Emmett-Teller (BET) and the Barret-Joyner-Hallender (BJH) methods, respectively. The external surface areas (S_{ext}) are evaluated by the t-plot method. The corresponding results are shown in Table-2, Figs. 4 and 5. From the results in Fig. 4, it is

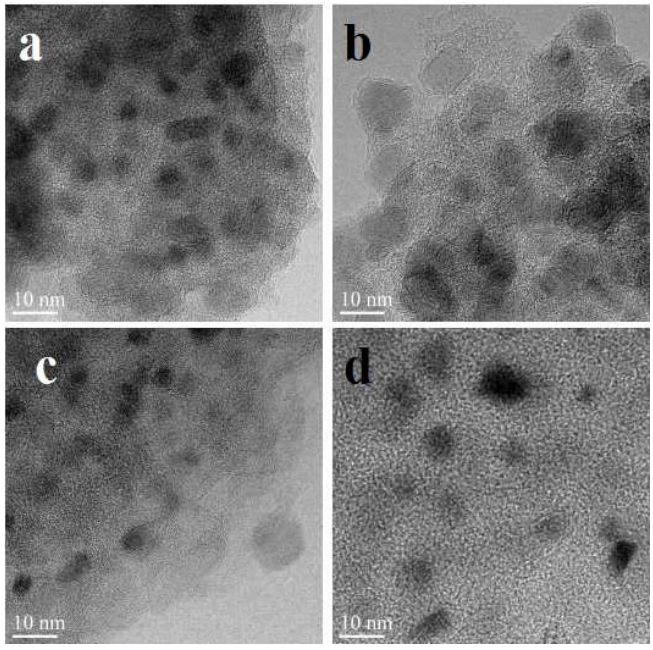

Fig. 3. TEM of the samples (a: TiO_2/C-600; b: TiO_2/C-700; c:TiO_2/C-800; d:TiO_2/C-900)

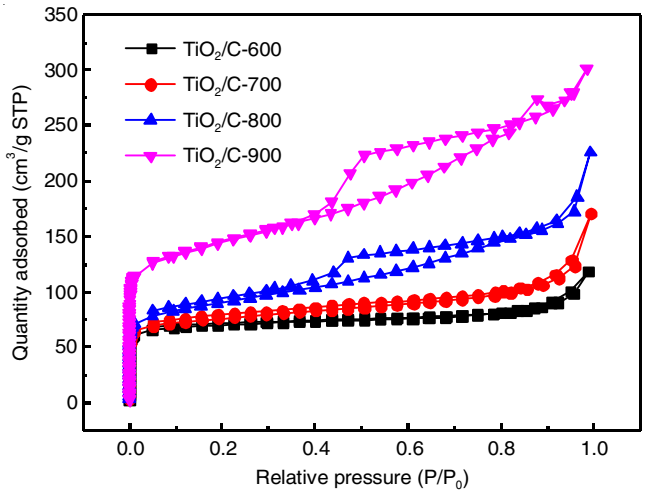

Fig. 4. N_2 adsorption-desorption isotherms of samples

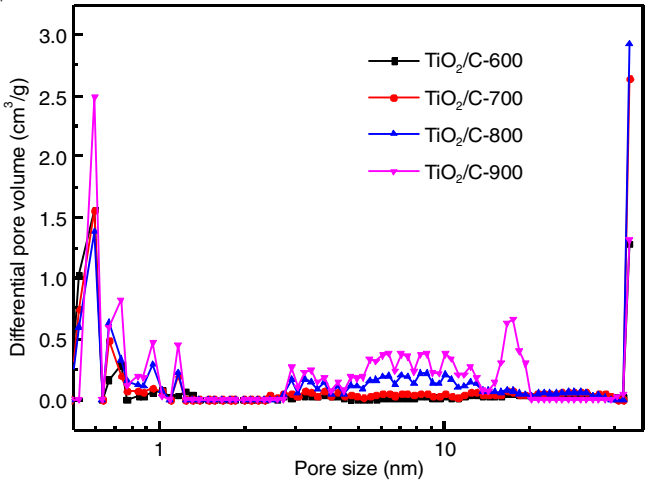

Fig. 5. Pore distribution images come from BJH models of the samples

TABLE-2
PORE STRUCTURE PARAMETERS OF THE SAMPLES

Samples	S_{BET} (m^2/g)	S_{ext} (m^2/g)	D_p (nm)	V_{mes}	V_{mic}
TiO_2/C-600	217.17	47.82	5.972	0.0932	0.0874
TiO_2/C-700	241.77	86.34	6.247	0.1837	0.0802
TiO_2/C-800	296.27	167.13	6.676	0.2919	0.0667
TiO_2/C-900	472.39	260.27	6.642	0.3766	0.1096

Notes: S_{BET}, surface area by a BET method; S_{ext}, external surface area by a t-plot method; D_p, the mean pore size evaluated by BJH pore size distribution curves from desorption branched of the N_2 adsorption isotherms; V_{mes}, pore volume of mesopores between 2 and 50 nm; V_{mic}, pore volume of micropores < 2 nm

clearly seen that all the isotherms exhibited a hysteresis loop near high p/p_0, characteristic of mesoporous and macroporous structure.

From the results in Table-2, it can be found that the specific surface areas of the synthesized aerogels increase with the increasing of the carbonization temperature under otherwise identical conditions. The specific surface area of the samples carbonization at 900 °C (472.39 m^2/g) is 1.6 times of the sample of carbonized at 800 °C . This is because in the process of carbonization the samples will shrink due to the high temperature, then the presence of TiO_2 will play a supporting role, so a high content of TiO_2 will enhance this role and the pore structure is not easy to collapse in the process of contraction. The high specific surface areas can improve the adsorption ability of the photocatalysts, because the photocatalytic activity strongly depends on the adsorption of organic substrate and the interfacial charge transfer can also be improved [17].

According to the existing provisions, the distribution of the microporous, macroporous and mesoporous is well divided [18]. From the results in Fig. 5 it is clear that the samples synthesized contain two kinds of pores (micro and mesopores). The area of micropores has the following order TiO_2/C-900 > TiO_2/C-800 > TiO_2/C-700 > TiO_2/C-600. The area in the mesopores has the following order TiO_2/C-900 > TiO_2/C-800 > TiO_2/C-700 > TiO_2/C-600.

In order to determine the chemical composition of the TiO_2/C nanocomposites, we used XPS analysis. Fig. 6 shows that the XPS survey spectra of the TiO_2/C nanocomposites. Fig. 6 shows a full scan spectrum of TiO_2/C nanocomposites. All peaks except one in spectrum (Fig. 6) belong to TiO_2. Two strongest peaks at 527 and 456 eV can be assigned to O1s and Ti2p excitations, respectively. The extra peak at 284 eV belongs to C1s. To analyze bonding nature of carbon atoms, focused scan was carried out around 284 eV, the result is plotted in Fig. 7. In Fig. 7, the C1s binding energy peaks are broad and asymmetric, suggesting that there are at least two kinds of C chemical states according to their binding energies ranging from 280 to 290 eV. After fitting of the curve, three peaks at binding energies of 284.6, 286.0 and 288.2 eV are clearly observed, indicating the existence of three different types of C states. The major peak at 284.6 eV could be assigned to adventitious carbon from the XPS instrument itself [19], whereas the other two minor peaks at 286.0 and 288.2 eV could be ascribed to the characteristic of the oxygen bound species C-O and C=O (or O-C-O) bonds [20,21], respectively. The peaks at 286.0 and 288.2 eV could suggest the formation

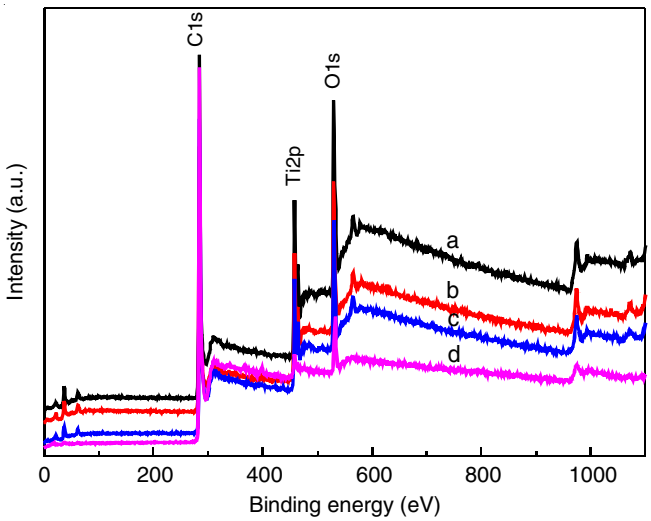

Fig. 6 XPS spectra of the samples (a: TiO_2/C-600; b: TiO_2/C-700; c:TiO_2/C-800; d:TiO_2/C-900)

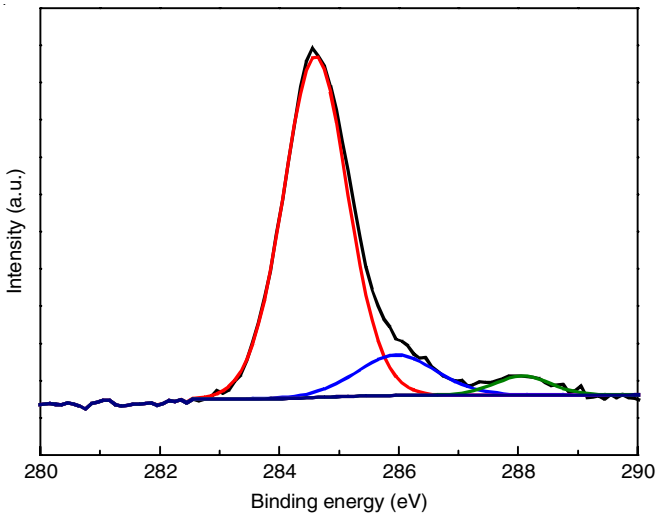

Fig. 7. XPS spectra of C1s TiO_2/C-900

of carbonate species and the substitution of Ti atom by C and formation of Ti-O-C structure, respectively, which can induce the narrowing of the band gap and response to visible light [22,23]. The peak around 282 eV is not observed, implying the absence of substitution of oxygen atom by carbon [24,25].

Fig. 8 shows the core level of the Ti2p spectrum of TiO_2/C nanocomposites. The core level binding energies of $Ti2p_{3/2}$ and $Ti2p_{1/2}$ in the TiO_2/C nanocomposite are 458.9 ± 0.2 eV and 464.6 ± 0.2 eV, respectively. By increasing the carbonization temperature, the peak positions of $Ti2p_{3/2}$ and $2p_{1/2}$ are found to be shifted toward low binding energy. However, the difference of 5.7 eV in all samples indicates the presence of the normal state of Ti^{4+} in the TiO_2 [26,27]. It might be explained by the interactions of Ti with oxygen vacancies [28]. As oxygen is a highly electronegative element, it withdraws the electron density from Ti. As a result, the binding energy of Ti in TiO_2/C nanocomposites increases with increasing of the oxygen vacancy concentration [29]. Then, when the carbonization temperature reaches 900 °C the peak shifted to 457.9 eV. This may be that Ti^{3+} appears in the samples at this carbonization temperature [30]. Under this carbonization condition the Ti

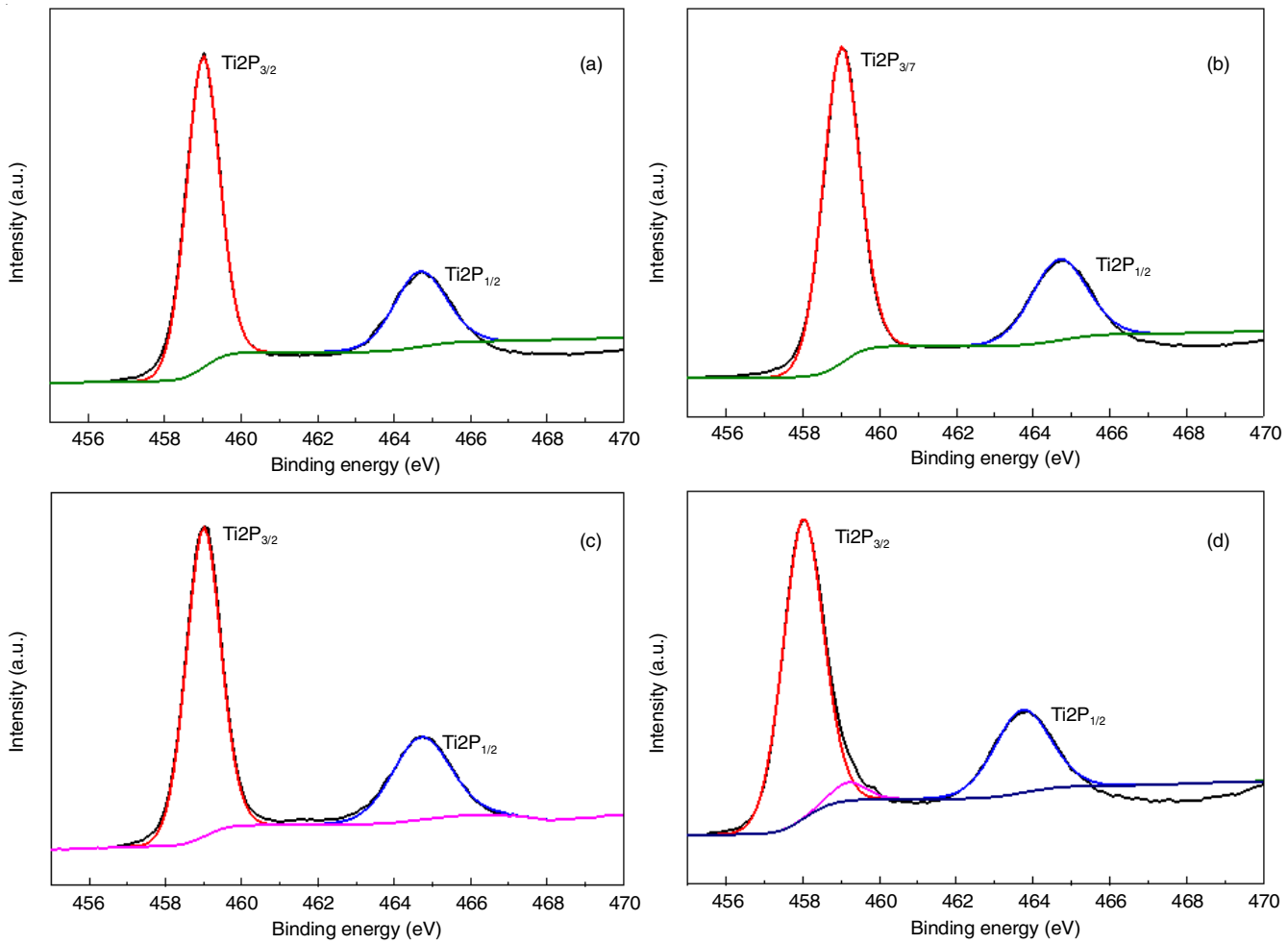

Fig. 8. $Ti2p_{3/2}$ and $Ti2p_{1/2}$ XPS spectra of TiO_2 (a: TiO_2/C-600; b: TiO_2/C-700; c:TiO_2/C-800; d:TiO_2/C-900)

state in the manner of both Ti^{3+} and Ti^{4+}, it could be of one of the reasons why the sample carbonized at 900 °C shows more excellent photocatalytic performance [30].

UV-visible absorptions of all samples are measured with a Jasco V-670 spectrophotometer from 200 to 800 nm and plotted in Fig. 9. From the Fig. 9A, it is observed that in the visible spectrum, with the carbonization temperature increasing, its absorption of visible light is also increased. Fig. 9B is the UV-visible diffuse reflectance spectra of the samples calcined under 800 °C in air. It is find that, after the samples calcined in air, the ability of visible light absorbance decreased greatly. This shows that the existence of carbon is advantageous to the samples for the absorption of visible light. And the visible light absorption of sample carbonized at 900 °C is better. This

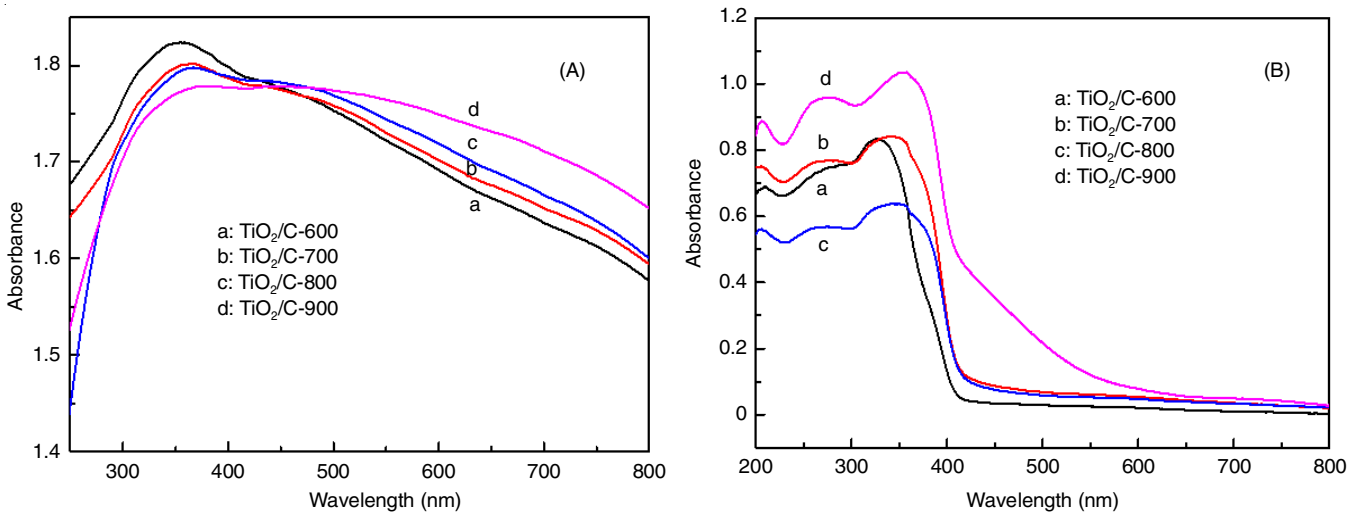

Fig. 9. UV-visible diffuse reflectance spectra of the four samples before calcination (A) and after calcination (B)

shows that the width of band gap of the sample is reduced. Their intention of the visible light absorption is in the order of TiO_2/C-900 > TiO_2/C-800 > TiO_2/C-700 > TiO_2/C-600.

Photocatalytic activity of different carbonization temperatures: To investigate the photocatalytic activities of the C-doped titania samples, photocatalytic degradation experiments are carried out using methylene blue in an aqueous suspension under visible light irradiation. Fig. 10 a) shows the results of the photocatalytic degradation of methylene blue in presence of different carbonized TiO_2/C hybrid aerogels for 200 min of irradiation. The different carbonized TiO_2/C photocatalysts exhibited higher photocatalytic degradation activities than pure TiO_2, indicating the promoting effect of the C modification. It has been reported in the literature that the photocatalytic activities of catalysts depend on many factors, such as crystallinity, surface properties, absorption properties, *etc.* [31]. In this case, the enhanced photocatalytic activity of TiO_2/C can be explained that the presence of C and the high carbonization temperature shifts the absorption edge to a longer wavelength in the order TiO_2/C-900 > TiO_2/C-800 > TiO_2/C-700 > TiO_2/C-600 (Fig. 9), which is in consistent with the order of the photocatalytic performances. A larger red shift indicates that the sample can absorb more photons. Therefore, the red shift in the absorption band is favourable for photocatalytic reaction.

To understand the reaction mechanism of methylene blue degradation, we applied the pseudo-first order model as expressed by the equation ln (C_0/C) = kt [where C_0 and C are the concentrations of methylene blue in solution at time 0 and t, respectively and t is the reaction time; k is the reaction rate constant (min^{-1})], which is generally used for photocatalytic degradation process [32], to treat the experimental data as depicted in Fig. 10a. The ln (C_0/C) s are plotted against t in Fig. 10b for P25, TiO_2/C-600, TiO_2/C-700, TiO_2/C-800 and TiO_2/C-900. The straight line indicates that the reaction kinetics is first order indeed for all samples. The reaction rate constants deduced from the slopes are 0.000143, 0.00418, 0.0107, 0.0207 and 0.0458 min^{-1} for P25, TiO_2/C-600, TiO_2/C-700, TiO_2/C-800 and TiO_2/C-900, respectively. The sample of TiO_2/C-900 shows the highest activity with a rate constant of 0.0458 min^{-1}. The high visible-light photocatalytic activity of TiO_2/C-900 can be attributed to the synergistic effects of high crystallinity of anatase phase, C-doping, high specific surface area and open mesoporous structure.

The above experiment shows that the samples play a significant role in the degradation of the basic dye methylene blue under visible light. In order to further understand whether the samples have a good photocatalytic degradation effect on acid dyes, we carry out the further experiments.

Fig. 11 shows the experimental data obtained by photocatalytic degradation of 50 mL, 10 mg/L methyl orange solution under visible light using 6.25 mg (A) and 12.5 mg (B) synthesized samples. As shown from this figure, they have a good degradation effect on methyl orange. The degradation effect of the sample carbonized at 900 °C on methyl orange is significantly higher than that of other samples. It obeys the following trend: TiO_2/C-900 > TiO_2/C-800 > TiO_2/C-700 > TiO_2/C-600 > P25. This phenomenon combined with some of the previous experimental data can be initially considered the sample TiO_2/C-900 not only has a higher titania content but also has a higher specific surface area than other samples. As we know, high titanium dioxide content can increase the efficiency of its photodegradation; at the same time, high specific surface area can increase the adsorption of dye molecules in the solution, which can also greatly improve the photodegradation efficiency.

It can be seen from Fig. 12 that the first-order kinetics model of degradation of methyl orange is similar to that of methylene blue. The samples which calcinated at the four carbonization temperatures are all in accordance with the first order kinetic model and the degrees of fit are all above 0.99. The reaction rate constant increases with the increase of carbonization temperature and this also shows that the reaction rate is growing. It can be shown that the efficiency of the samples in the photocatalytic effect increases with the carbonization temperature increasing, which is advantageous in practical production applications.

Conclusions

TiO_2/C hybrid aerogels were successfully synthesized by sol-gel method and treated by the supercritical drying

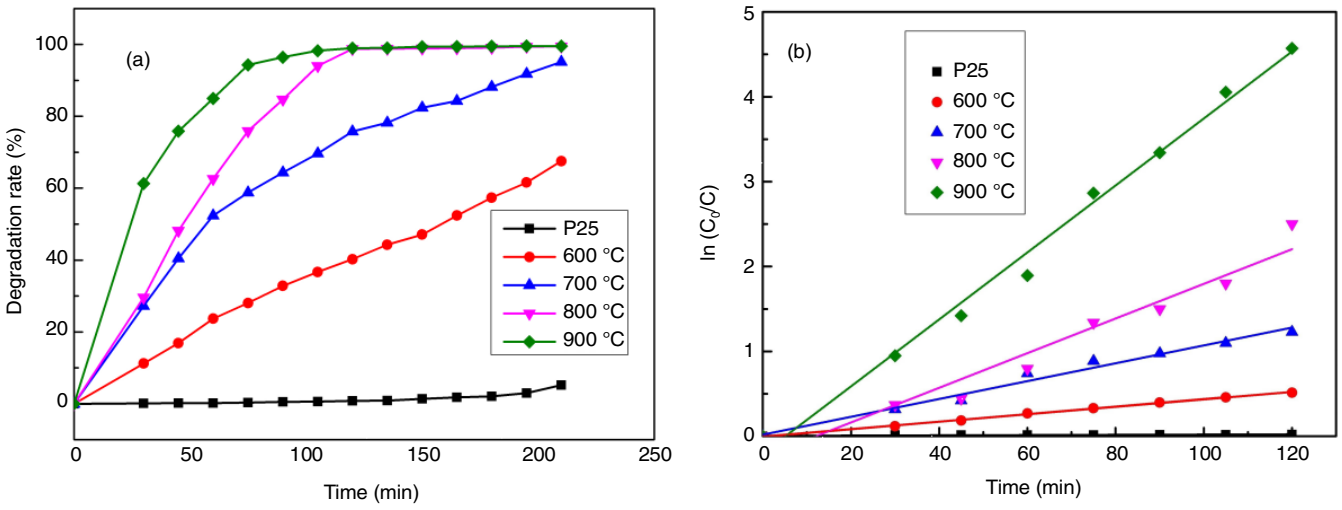

Fig. 10. (a) Photocatalytic degradation of methylene blue under the visible light, (b) First order kinetic model of photocatalytic degradation of methylene blue

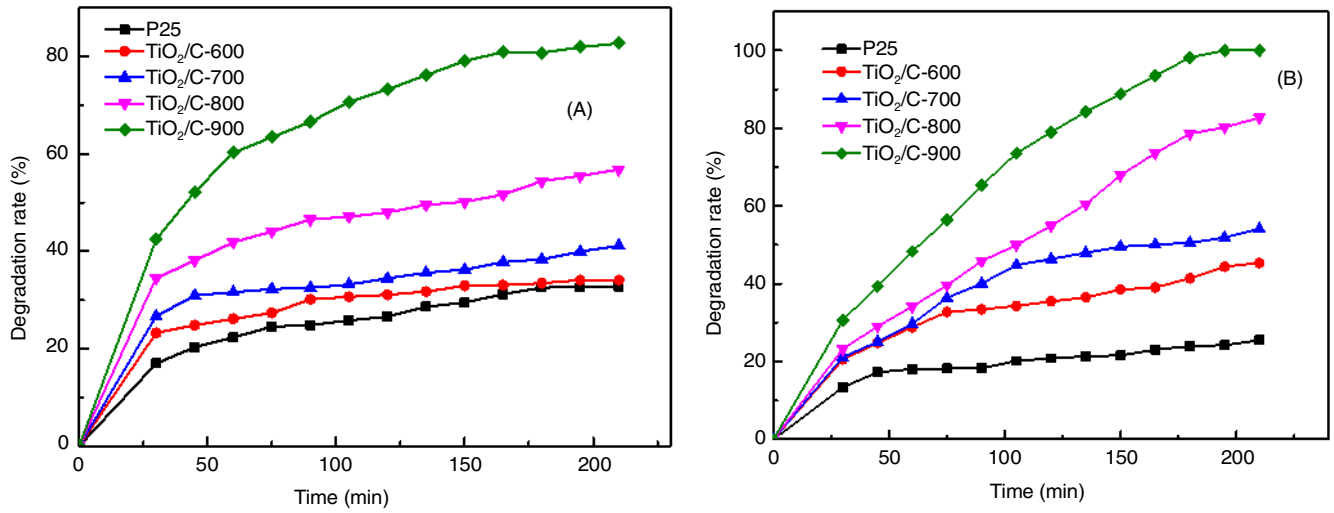

Fig. 11. Photocatalytic degradation of methyl orange under the visible light with different content of the samples (A) 6.25 mg and (B) 12.5 mg

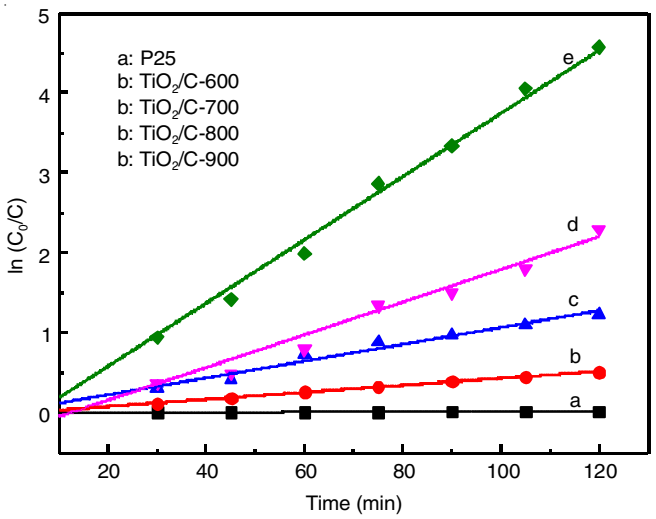

Fig. 12. First-order kinetics fitting curve for photocatalytic degradation of methyl orange

method then carbonized under different temperatures (600, 700, 800, 900 °C). The effects of the carbonization temperature on the crystal phase, morphology, specific surface area and porous property, optical response property of the resultant samples were investigated in detail. Several important facts were disclosed as follows:

(1) XRD revealed that precursor $TiCl_4$ can be transformed into anatase TiO_2 completely after sol-gel, supercritical drying and carbonization at different temperatures. SEM demonstrated that TiO_2 nanoparticles are highly porous material and the size of nanoparticles increased with the enhancement of carbonization temperature. BET analysis disclosed that the specific surface areas of the synthesized samples were significantly improved as the carbonization temperature increasing. XPS analysis demonstrated that the doping of carbon occurred during the experimentation. UV-visible absorption showed that TiO_2/C presented red-shift absorption edge and exhibited strong absorption in the visible region.

(2) Compared with pure TiO_2, the obtained TiO_2/C presented more excellent visible-light photocatalytic activity for the decoloration of methylene blue and methyl orange, which could be attributed to the crucial factor, high specific surface area of TiO_2/C. TiO_2/C-900 °C presented optimal visible-light photocatalytic activity with a high reaction rate constant (0.0458 min^{-1}) among the four TiO_2/C samples, which was much higher than some previously reported results.

ACKNOWLEDGEMENTS

This work was supported by the Capacity Building Program of Shanghai Local Universities (No. 12160503600), the First-Class Discipline Construction Fund of Shanghai Municipal Education Commission (No. J201212), Nature Science Foundation of China (U1332107) and Key Discipline Construction Fund of Composite Materials of Shanghai Institute of Technology (No. 10210Q140001).

REFERENCES

1. J.L. Gole, J.D. Stout, C. Burda, Y. Lou and X. Chen, *ChemInform*, **35**, 1230 (2004); https://doi.org/10.1002/chin.200417021.
2. L. Baia, L. Diamandescu, L. Barbu-Tudoran, A. Peter, G. Melinte, V. Danciu and M. Baia, *J. Alloys Comp.*, **509**, 2672 (2011); https://doi.org/10.1016/j.jallcom.2010.11.154.
3. M.M. Higarashi and W.F. Jardim, *Catal. Today*, **76**, 201 (2002); https://doi.org/10.1016/S0920-5861(02)00219-5.
4. P.V.R.K. Ramacharyulu, G.K. Prasad, K. Ganesan and B. Singh, *J. Mol. Catal. Chem.*, **353–354**, 132 (2012); https://doi.org/10.1016/j.molcata.2011.11.016.
5. T. An, W. Zhang, X. Xiao, G. Sheng, J. Fu and X. Zhu, *J. Photochem. Photobiol. Chem.*, **161**, 233 (2004); https://doi.org/10.1016/j.nainr.2003.08.004.
6. C. Wang, Y. Ao, P. Wang, J. Hou and J. Qian, *Powder Technol.*, **210**, 203 (2011); https://doi.org/10.1016/j.powtec.2011.03.015.
7. J. Liu, W. Qin, S. Zuo, Y. Yu and Z. Hao, *J. Hazard. Mater.*, **163**, 273 (2009); https://doi.org/10.1016/j.jhazmat.2008.06.086.
8. S. Rengaraj, S. Venkataraj, J.W. Yeon, Y. Kim, X.Z. Li and G.K.H. Pang, *Appl. Catal. B*, **77**, 157 (2007); https://doi.org/10.1016/j.apcatb.2007.07.016.
9. F.E. Osterloh, *ChemInform*, **39**, 35 (2008); https://doi.org/10.1002/chin.200813223.
10. D. Chen, Z. Jiang, J. Geng, Q. Wang and D. Yang, *Ind. Eng. Chem. Res.*, **46**, 2741 (2007); https://doi.org/10.1021/ie061491k.
11. P. Górska, A. Zaleska, E. Kowalska, T. Klimczuk, J.W. Sobczak, E. Skwarek, W. Janusz and J. Hupka, *Appl. Catal. B*, **84**, 440 (2008); https://doi.org/10.1016/j.apcatb.2008.04.028.

12. Z. Zhang, L. Zhang, M.N. Hedhili, H. Zhang and P. Wang, *Nano Lett.*, **13**, 14 (2013); https://doi.org/10.1021/nl3029202.
13. D. Sun, K. Wang, Z. Xu and R. Li, *J. Rare Earths*, **33**, 491 (2015); https://doi.org/10.1016/S1002-0721(14)60446-4.
14. T. Tsumura, N. Kojitani, I. Izumi, N. Iwashita, M. Toyoda and M. Inagaki, *J. Mater. Chem.*, **12**, 1391 (2002); https://doi.org/10.1039/b201942f.
15. M.L. Chen, C.S. Lim and W.C. Oh, *J. Ceram. Process. Res.*, **8**, 119 (2007).
16. M. Inagaki, F. Kojin, B. Tryba and M. Toyoda, *Carbon*, **43**, 1652 (2005); https://doi.org/10.1016/j.carbon.2005.01.043.
17. L. Pan, J.J. Zou, X. Zhang and L. Wang, *J. Am. Chem. Soc.*, **133**, 10000 (2011); https://doi.org/10.1021/ja2035927.
18. M.S. Hamdy, R. Amrollahi and G. Mul, *ACS Catal.*, **2**, 2641 (2012); https://doi.org/10.1021/cs300593d.
19. W. Ren, Z. Ai, F. Jia, L. Zhang, X. Fan and Z. Zou, *Appl. Catal. B*, **69**, 138 (2007); https://doi.org/10.1016/j.apcatb.2006.06.015.
20. D. Li, Z. Xing, X. Yu and X. Cheng, *Electrochim. Acta*, **170**, 182 (2015); https://doi.org/10.1016/j.electacta.2015.04.148.
21. V. Kiran and S. Sampath, *ACS Appl. Mater. Interfaces*, **4**, 3818 (2012); https://doi.org/10.1021/am300349k.
22. H. Wang, Z. Wu and Y. Liu, *J. Phys. Chem. C*, **113**, 13317 (2009); https://doi.org/10.1021/jp9047693.
23. Y. Zhang, Z. Zhao, J. Chen, L. Cheng, J. Chang, W. Sheng, C. Hu and S. Cao, *Appl. Catal. B*, **165**, 715 (2015); https://doi.org/10.1016/j.apcatb.2014.10.063.
24. J. Yu, Q. Li, S. Liu and M. Jaroniec, *Chem. Eur. J.*, **19**, 2433 (2013); https://doi.org/10.1002/chem.201202778.
25. W. Qian, P.A. Greaney, S. Fowler, S.-K. Chiu, A.M. Goforth and J. Jiao, *ACS Sustain. Chem. Eng.*, **2**, 1802 (2014); https://doi.org/10.1021/sc5001176.
26. S. Lee, Y. Lee, D.H. Kim and J.H. Moon, *ACS Appl. Mater. Interfaces*, **5**, 12526 (2013); https://doi.org/10.1021/am403820e.
27. F. He, F. Ma, J. Li, T. Li and G. Li, *Ceram. Int.*, **40**, 6441 (2014); https://doi.org/10.1016/j.ceramint.2013.11.094.
28. S. Sharma, S. Chaudhary, S.C. Kashyap and S.K. Sharma, *J. Appl. Phys.*, **109**, 083905 (2011); https://doi.org/10.1063/1.3567938.
29. F. Dong, S. Guo, H. Wang, X. Li and Z. Wu, *J. Phys. Chem. C*, **115**, 13285 (2011); https://doi.org/10.1021/jp111916q.
30. J.P. Espinós, A. Fernández and A.R. González-Elipe, *Surf. Sci. Lett.*, **295**, 402 (1993); https://doi.org/10.1016/0039-6028(93)90287-T.
31. M. Saif and M.S.A. Abdel-Mottaleb, *Inorg. Chim. Acta*, **360**, 2863 (2007); https://doi.org/10.1016/j.ica.2006.12.052.
32. J.W. Shi, C. Liu, C. He, J. Li, C. Xie, S. Yang, J.-W. Chen, S. Li and C. Niu, *RSC Adv.*, **5**, 17667 (2015); https://doi.org/10.1039/C4RA15824E.